AGU PUBLICATIONS

Space Weather

RESEARCH ARTICLE
10.1002/2016SW001481

Special Section:
Sun to Earth: Heliospheric Remote Sensing Observations Applicable to Space Weather

Key Points:
- Investigation of SOLIS and GONG data sets and their extrapolation to Earth in situ measurements using the UCSD IPS tomography technique
- Comparison of "closed" (near-Sun) fields with those at Earth
- Comparison of CSSS and PFSS model closed fields

Correspondence to:
B. V. Jackson,
bvjackson@ucsd.edu

Citation:
Jackson, B. V., H.-S. Yu, A. Buffington, P. P. Hick, N. Nishimura, N. Nozaki, M. Tokumaru, K. Fujiki, and K. Hayashi (2016), Exploration of solar photospheric magnetic field data sets using the UCSD tomography, *Space Weather*, *14*, 1107–1124, doi:10.1002/2016SW001481.

Received 30 JUL 2016
Accepted 22 OCT 2016
Accepted article online 26 OCT 2016
Published online 10 DEC 2016

Exploration of solar photospheric magnetic field data sets using the UCSD tomography

B. V. Jackson[1], H.-S. Yu[1], A. Buffington[1], P. P. Hick[1], N. Nishimura[2], N. Nozaki[2], M. Tokumaru[2], K. Fujiki[2], and K. Hayashi[2]

[1]Center for Astrophysics and Space Sciences, University of California, San Diego, La Jolla, California, USA, [2]Institute for Space-Earth Environmental Research, Nagoya University, Nagoya, Japan

Abstract This article investigates the use of two different types of National Solar Observatory magnetograms and two different coronal field modeling techniques over 10 years. Both the "open-field" Current Sheet Source Surface (CSSS) and a "closed-field" technique using CSSS modeling are compared. The University of California, San Diego, tomographic modeling, using interplanetary scintillation data from Japan, provides the global velocities to extrapolate these fields outward, which are then compared with fields measured in situ near Earth. Although the open-field technique generally gives a better result for radial and tangential fields, we find that a portion of the closed extrapolated fields measured in situ near Earth comes from the direct outward mapping of these fields in the low solar corona. All three closed-field components are nonzero at 1 AU and are compared with the appropriate magnetometer values. A significant positive correlation exists between these closed-field components and the in situ measurements over the last 10 years. We determine that a small fraction of the static low-coronal component flux, which includes the Bn (north-south) component, regularly escapes from closed-field regions. The closed-field flux fraction varies by about a factor of 3 from a mean value during this period, relative to the magnitude of the field components measured in situ near Earth, and maximizes in 2014. This implies that a relatively more efficient process for closed-flux escape occurs near solar maximum. We also compare and find that the popular Potential Field Source Surface and CSSS model closed fields are nearly identical in sign and strength.

1. Introduction

An important goal of current heliospheric physics is a reconstruction of the coronal and heliospheric magnetic field using extrapolations from photospheric magnetic field observations. This endeavor is important for accurate prediction of geomagnetic storms, which are often produced when the southward solar magnetic field arrives at Earth and couples with the Earth's magnetic field [e.g., *Kamide et al.*, 1997; *Russell*, 2001]. The Stanford Potential Field Source Surface (PFSS) model [e.g., *Schatten et al.*, 1969; *Hoeksema et al.*, 1983], the Current-Sheet Source-Surface (CSSS) model [*Zhao and Hoeksema*, 1995], and other more sophisticated types of models have been used to extrapolate magnetic fields into the corona. Many of these models including the PFSS and CSSS models have been used to extrapolate slow changes in the solar surface magnetic field (on the order of several days or more) into the heliosphere. For instance, the PFSS model is used in the Wang-Sheely-Arge (WSA) propagation model [*Arge and Pizzo*, 2000] and implemented by NOAA in operational space weather forecasts. Even more sophisticated models such as those using three-dimensional magnetohydrodynamics (3-D MHD) [e.g., *Riley et al.*, 2011] are used to link surface fields into the heliosphere and then extrapolate outward to those observed in situ. The reader is referred to *Mackay and Yeates* [2012] for a more comprehensive model review.

Since the middle of the last decade we have used National Solar Observatory (NSO) Synoptic Optical Long-term Investigations of the Sun (SOLIS) photospheric magnetic field measurements [*Keller et al.*, 2003a, 2003b] extrapolated outward from the Sun and have compared these results with in situ observations from spacecraft. Synoptic maps, updated daily from compilations of photospheric magnetograms, are used to calculate a radial source-surface magnetic field at 15 Rs using the CSSS model. Beyond this source surface, the magnetic field is convected along velocity flow lines [*Dunn et al.*, 2005; *Jackson et al.*, 2012] derived by a tomographic technique developed at the University of California, San Diego, (UCSD) [see *Jackson et al.*, 2011, and references therein] applied to interplanetary scintillation (IPS) observations (for early IPS references see *Hewish et al.* [1964] and *Houminer* [1971]) (see Figure 1). IPS data used in the present paper are from the

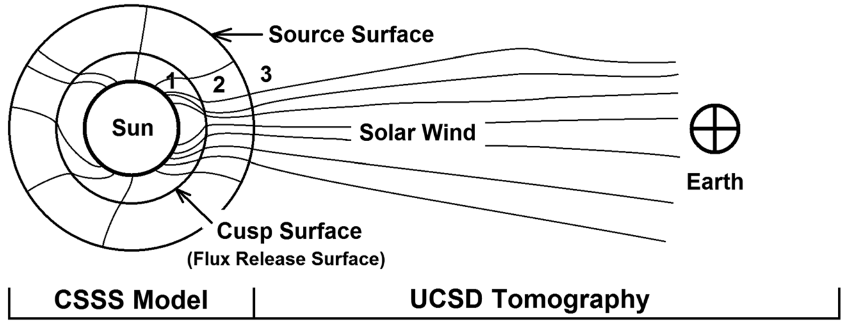

Figure 1. In the inner region (1), the CSSS model calculates the magnetic field using solar photospheric magnetograms. In the middle region (2), the CSSS model opens the field lines by imposing a horizontal current at the cusp surface. In the outer region (3), the UCSD 3-D tomography extrapolates the magnetic field along velocity flow lines [*Dunn et al.*, 2005].

Solar Terrestrial Environment Laboratory (STELab), now called the Institute for Space-Earth Environmental Research (ISEE), Japan [*Kojima and Kakinuma*, 1987]. To further refine these results, the analyses are fit to near-Earth in situ measurements of plasma velocities and densities [*Jackson et al.*, 2010, 2013]. Global heliospheric results are calculated for Carrington rotation time intervals (27 days). With IPS observations available in real time, conditions at 1 AU can be predicted several days in advance.

SOLIS magnetograms, as input to the CSSS model (see section 3), have regularly given good results [*Jackson et al.*, 2012] compared with near-Earth measured in situ radial and tangential fields. Although we have not used NSO Global Oscillation Network Group (GONG) observations (http://gong.nso.edu/data/magmap/) previously, we want to determine whether they provide as good or better near-Earth magnetic-field extrapolations. Additionally, in a recent study, *Jackson et al.* [2015] used SOLIS magnetograms and the CSSS model to extrapolate fields from below the cusp surface (hereafter termed as "closed-field" analyses) radially upward over a period of 3 years and found that these have shown positive correlations with the north-south flux component measured in situ. These analyses (or see *Yeates et al.* [2010]) also suggest that even better resolved in situ extrapolations may be thus obtained from this type of extrapolation and that these may include the fields present around coronal mass ejections (CMEs) [e.g., *Owens et al.*, 2008] and especially at their onsets [e.g., *Wu et al.*, 2015a, 2015b; *Nishimura et al.*, 2016; *Nozaki et al.*, 2016]. With these results in hand, we have been motivated to provide a more complete study of the CSSS model and its use for extrapolating magnetic fields with both the open- and closed-field techniques.

Section 2 of this article provides a background of the tomographic technique and how the data sets are used in these extrapolations. Section 3 details the 10 year study that correlates the open-field radial and tangential CSSS model SOLIS and GONG extrapolations with both Advanced Composition Explorer (ACE) [*Stone et al.*, 1998] and Wind [*Ogilvie and Parks*, 1996] in situ magnetic fields. Section 4 is a similar CSSS model closed-field analysis that compares these with ACE and Wind data sets. In section 5 we discuss these results, and we conclude in section 6.

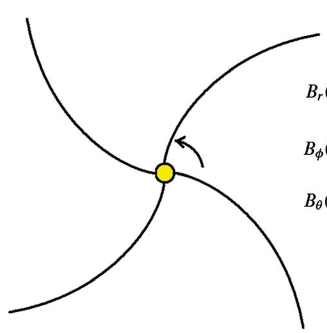

$$B_r(r,\phi,\theta) = B(r_0,\phi_0,\theta_0)\left(\frac{r_0}{r}\right)^2$$

$$B_\phi(r,\phi,\theta) = -B(r)\left(\frac{\omega r_0 \sin(\theta)}{V}\right)\left(\frac{r_0}{r}\right)$$

$$B_\theta(r,\phi,\theta) = 0$$

Figure 2. In the heliosphere beyond the CSSS model source surface, the rotating Sun provides a spiral field that approximately follows the equations given above as structures flow nearly radially outward.

2. Tomographic Analysis and Field Extrapolation Using a Sample Data Set

The UCSD and ISEE heliospheric groups separately developed iterative Computer Assisted Tomography (CAT) programs [*Kojima et al.*, 1998; *Jackson et al.*, 1998, 2003, 2011] to provide better resolution (or differentiation) of separate heliospheric structures that are viewed by remotely sensed IPS observations. Both analyses fit the IPS observations to a

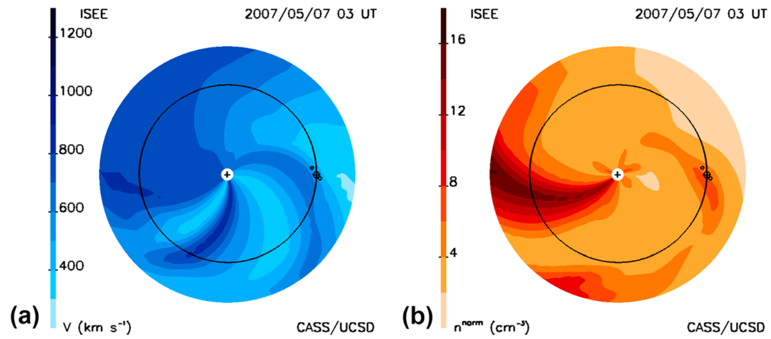

Figure 3. Ecliptic cuts showing (a) radial velocity and (b) proton density from the ISEE data on 7 May 2007 at 3 UT. Earth is to the right in each image shown on its orbit. The two small circles near Earth are the locations of Solar Terrestrial Relations Observatory satellites (STEREO) A (top) and STEREO B (bottom) at that time.

model of the heliosphere and then extract global information from that model. Originally, both analyses provided this differentiation using rotational tomography similar to a CAT scan where the object is rotated and the view of it remains fixed. However, anticipating abundant Thomson scattering data availability from the Solar Mass Ejection Imager (SMEI) instrument [*Jackson et al*., 2004] on board the Earth-orbiting Coriolis spacecraft, a time-dependent version of the tomography program was developed [*Jackson et al*., 2001]. This revision enabled the reconstruction of both CMEs and corotating heliospheric structures by fitting remotely sensed observations to a kinematic model that conserved mass and mass flux. In this analysis, the change in line-of-sight (LOS) weighting and the kinematic flux constraints are the primary way in which structures are

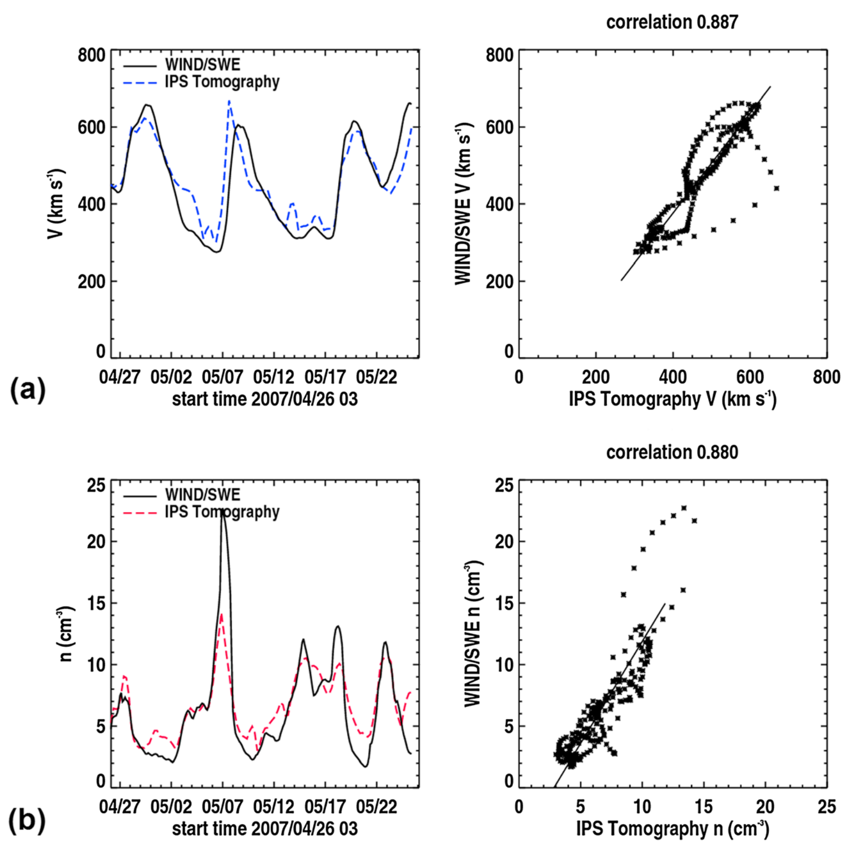

Figure 4. Time series (left panels) from the IPS 3-D reconstructions (dashed lines) compared with ACE SWEPAM level 0 measurements over the same Carrington rotation 2056 time period. Correlations are in the right panels. The in situ measurements have been smoothed by a 1 day "boxcar" filter to provide a signal commensurate with the 1 day cadence of the tomographic analysis. (a) Radial velocity and (b) proton density.

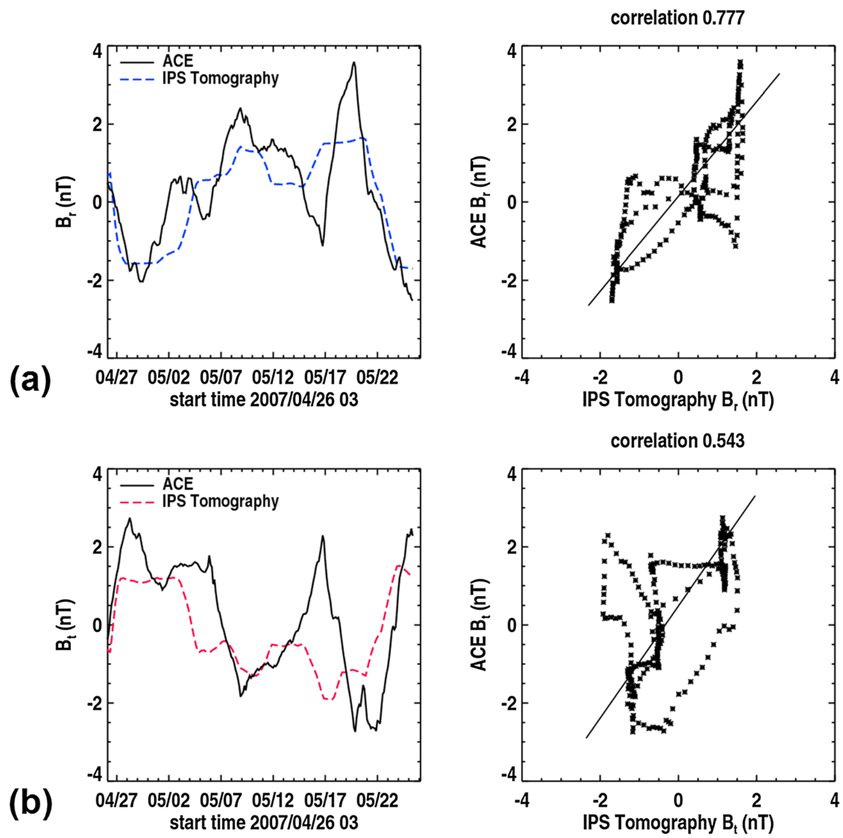

Figure 5. Time series (left) and correlations (right) from the CSSS open-field modeling and IPS 3-D reconstruction extrapolations of GONG data compared with ACE magnetometer measurements over the same Carrington rotation 2056 time period. The in situ measurements have been smoothed by a 3 day boxcar filter to provide a signal commensurate with the smoothed measurements from the CSSS modeling. (a) Radial fields and (b) tangential fields.

differentiated along the LOS [see *Jackson et al*., 2011, 2015; *Yu et al*., 2015]. In the UCSD tomographic analysis, scintillation level when viewing distant point sources is used as a proxy for density along the LOS. This and velocity perpendicular to the line of sight are fit to the kinematic solar wind model to provide global 3-D maps of velocities and densities.

Only a few thousand LOS exist in any given solar rotation from the current ISEE data sets, and this limits the spatial and temporal resolution: the results are smoothed with a Gaussian spatial and temporal filter to about $20° \times 20°$ in latitude and longitude and a 1 day temporal cadence. All LOS available for the reconstructions emanate from Earth are thus more numerous near the Earth and are thus better able to reconstruct nearby structures. Even so, this resolution suffices to determine the large-scale features of CME velocity and density structure. This analysis converges well: after a few iterations any information from the initial distribution has died away. The technique has successfully analyzed CME-associated velocity and density structures using both IPS and Thomson scattering observations (for a review see *Jackson et al*. [2011]). UCSD reconstruction analyses of IPS data compare favorably with ISEE results [*Tokumaru*, 2013; *Jackson et al*., 2011]. For mathematical details about the UCSD CAT program, see *Hick and Jackson* [2004] and *Jackson et al.* [2008].

The UCSD time-dependent CAT program recently incorporated inclusion of near-Earth in situ data for LOS analyses [*Jackson et al*., 2010, 2013]. This process adds highly weighted values of in situ measurements at L_1 to the closest near-Earth LOS segment. The result is a better determined prediction of the *change* from current in situ plasma conditions. Additionally, we found [*Jackson et al*., 2010] that this provided a globally more uniform time-dependent reconstruction. Considering a column extending from the sub-Earth point on the Sun to the Earth, the results match in situ values of velocity and density well, all the while maintaining the kinematic mass and mass flux conservation. This is important when extrapolating the magnetic field components from the source surface, since it provides an accurate timing for the entrained magnetic flux going

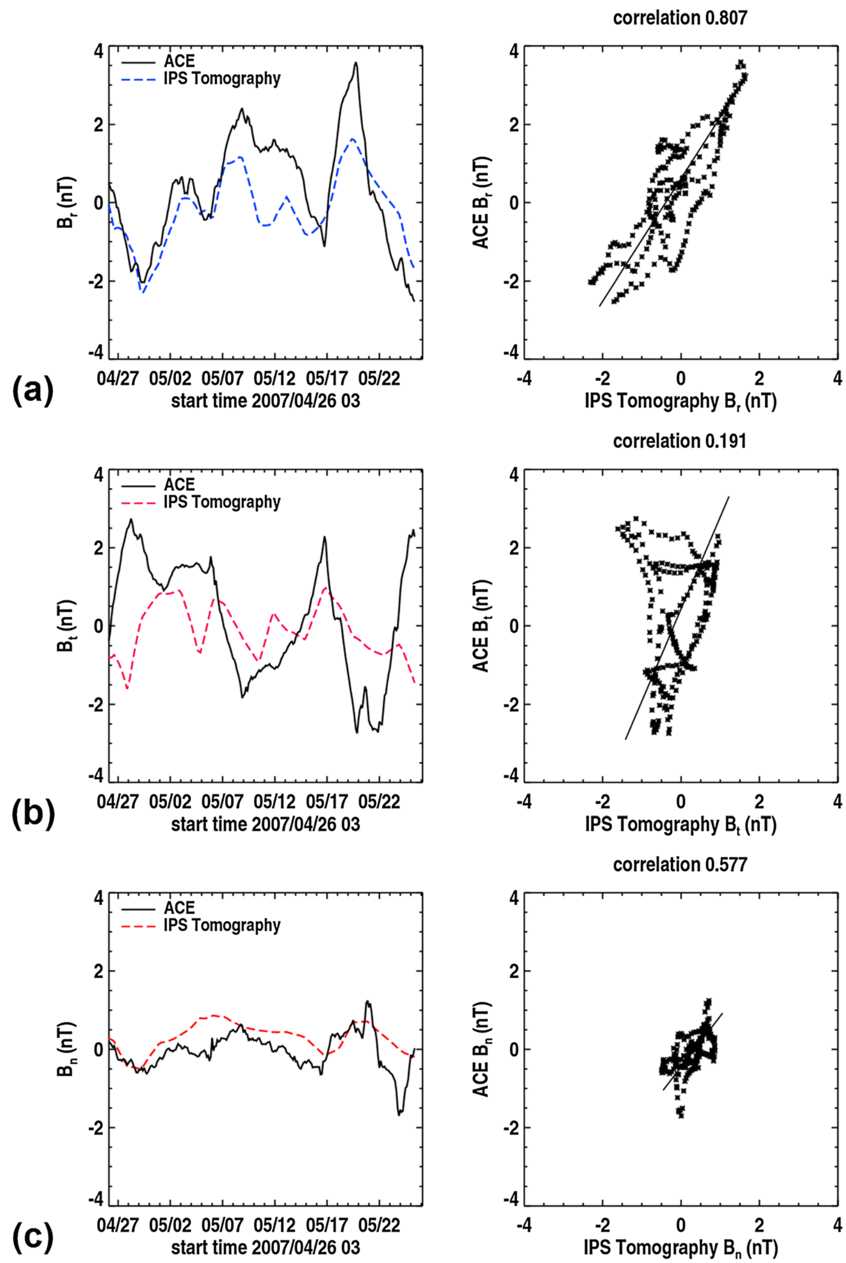

Figure 6. Time series (left) and correlations (right) from the CSSS closed-field modeling at 1.3 Rs and IPS 3-D reconstruction extrapolations of GONG data compared with ACE magnetometer measurements over the same Carrington rotation 2056 time period. The in situ measurements have been smoothed by a 3 day boxcar filter to provide a signal commensurate with the smoothed measurements from the CSSS modeling. (a) Radial fields, (b) tangential fields, and (c) normal fields.

from this source surface to Earth. Inclusion of this extra in situ data near Earth, but keeping the same numbers of lines of sight, also permits twice finer latitude and longitude resolution and half a day temporal cadence.

The radial velocities provided by the UCSD time-dependent tomography program are used in the magnetic field calculations above the CSSS model source surface as shown in Figure 2. Since the plasma has a high electrical conductivity, we assume that beyond the source surface, the magnetic field is frozen into the plasma [*Alfvén*, 1942; *Hundhausen*, 1972] and follows the velocity flow lines. In Figure 2 r, φ, and θ are heliographic radial, tangential, and latitudinal (RTN) coordinates, and $B(r_0, \varphi_0, \theta_0)$ is the magnitude of the magnetic field at the 15 Rs source surface of the CSSS model. When employed in the usual way, the CSSS-derived fields are assumed to corotate out to the source surface (15 Rs), and, at that location, are

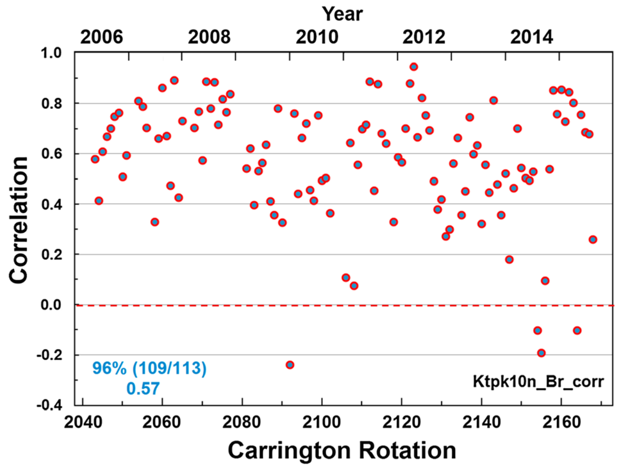

Figure 7. Pearson's *R* correlations for the radial (Br) field from CSSS open-field model SOLIS data analysis extrapolated to Earth and compared with ACE in situ observations.

strictly radial as enforced by the modeling. The radial field provides a tangential component by solar rotation ω, in radians s^{-1}. In these analyses we use $V = V(r, \varphi, \theta)$ from the tomography as the relevant outflow velocity at location (r, φ, θ) in the heliosphere. From the source surface, the tangential field B_φ is produced by solar rotation at large distances from the source surface. $B(r_0, \varphi_0, \theta_0)$ varies in time relative to a fixed point in space or to Earth moving slowly in its orbit as the values of the magnetic field strengths change due to solar rotation past Earth or the evolution of solar surface magnetic structures. Note, in this analysis, that the magnetic field component (B_θ) normal to the solar rotation is identically zero.

Figure 3 shows a sample of the global tomographic analysis of velocity and density using the time-dependent tomography as ecliptic cuts at the indicated date and time. These show that the global speeds in km s^{-1} and densities that have been calibrated relative to proton numbers and presented with an r^{-2} radial falloff relative to the values at 1 AU. The dense structure at Earth is probably associated with a wide angle CME observed in Large Angle and Spectrometric Coronagraph images that erupted from near the center of the Sun on 2 May 2007 at ~19:00 UT and moved outward to the west of the Sun-Earth line on the next day. The velocity data of Figure 3 shows that this density is followed by a corotating high-speed stream. Figure 4 shows the time series analyses of velocity and density for Carrington rotation 2056 that includes this period obtained from the volumetric data near Earth. These are compared with the ACE spacecraft Solar Wind Electron Proton Alpha Monitor (SWEPAM) [*McComas et al.*, 1998] level 0 measurements. Comparisons here and in subsequent figures are also shown employing Pearson's "*R*" correlation (see §13.7 in *Press et al.*, (1988)). During this 27 day period near solar minimum, there are variations in radial velocity, and density present over the interval that is generally associated with corotating heliospheric structures.

Figure 5 shows extrapolated radial and tangential magnetic fields for Carrington rotation 2056 as given by CSSS open-field modeling where radial fields are imposed on the 15 Rs source surface from GONG magnetogram data. This analysis uses the Figure 2 equations and is extrapolated outward from the 15 Rs source surface: its results are compared with ACE magnetometer measurements (see http://helios.gsfc.nasa.gov/ace/mag.html) in RTN coordinates. Considerable work went into choosing the proper parameters for the CSSS model, both by *Zhao and Hoeksema* [1995] and when first used with the UCSD tomography model by *Dunn et al.* [2005]. Here the cusp surface is at 1.6 Rs, the source surface is at 15 Rs, and $n = 9$ expansion

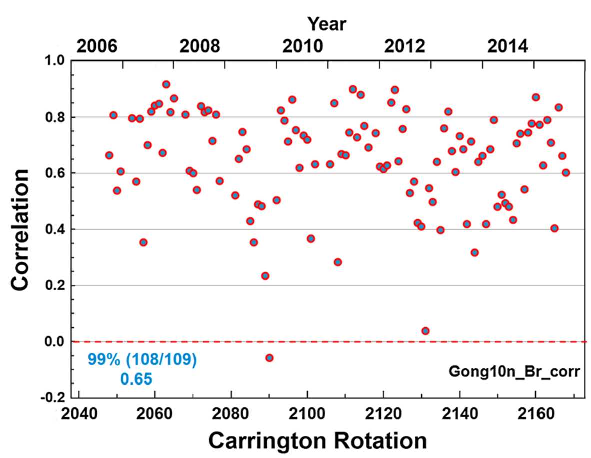

Figure 8. Correlations for the radial (Br) field from CSSS open-field model GONG data analysis radial extrapolated to Earth and compared with ACE in situ measurements.

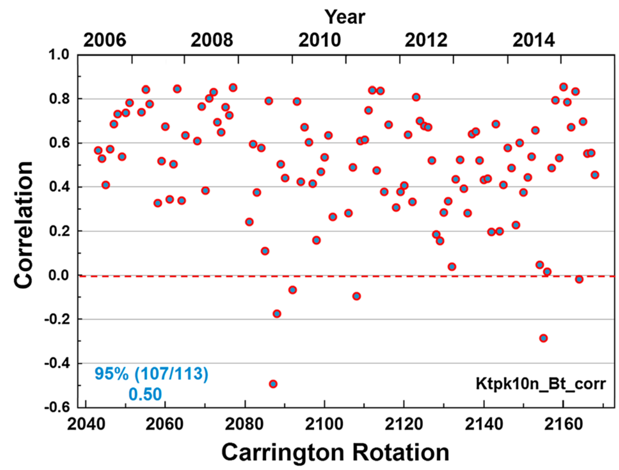

Figure 9. Correlations for the tangential (Bt) field from CSSS open-field model SOLIS data analysis extrapolated to Earth and compared with ACE in situ measurements.

coefficients are unchanged since that time. The current employed at the cusp surface to provide the radial fields is also as in the original *Zhao and Hoeksema* [1995] modeling and is not varied over time. These values are also used for the CSSS closed-field analyses, except for employing $n = 20$ expansion coefficients. Although $n = 20$ provides more structure near the solar surface, only an insignificant change occurs near the cusp surface at 1.6 Rs or in the open-field result at the source surface. *Dunn et al.* [2005] experimented with changing the location of the source surface from 15 Rs down to 2.5 Rs for over a year's worth of analyses, and this too did not significantly change modeled in situ correlations. We settled on 15 Rs because it is the approximate solar distance of the Alfvén surface, and here much of the solar wind acceleration has already taken place.

The CSSS closed fields modeled in this analysis are extrapolated outward radially from 1.3 Rs to the 15 Rs source surface. All three field components are present below the CSSS model cusp surface at 1.6 Rs. The extrapolation to 15 Rs employs an $r^{-1.34}$ falloff (see below) from 1.3 Rs. From that point onward, two choices about the falloff of the three components are needed so that their strengths match in situ values. The first assumption is that the fields near the solar surface are static and that only a small portion (2%) of these fields participates in the outward component expansion. Following this, a choice needs to be made of the radial falloff to be associated with each component. For the radial and tangential closed fields we use the assumption that these fields follow the equations of Figure 2. The normal (Bn) falloff is not specified in Figure 2, but we know that an approximate falloff from 0.3 AU outward to 1 AU is $r^{-1.34\pm0.10}$ from Helios spacecraft magnetometer observations [*Mariani and Neubauer*, 1990]. Using this falloff upward from the source surface at 15 Rs sets the

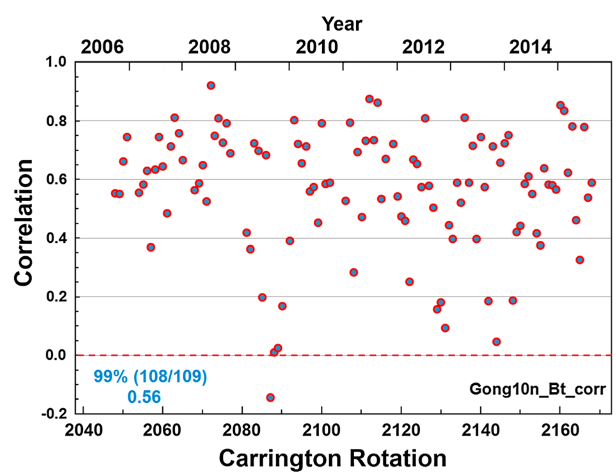

Figure 10. Correlations for the tangential (Bt) field from CSSS model GONG data analysis extrapolated to Earth and compared with ACE in situ measurements.

Table 1. CSSS Model Open-Field Extrapolation and Correlation Comparison

Comparison	Average Correlation	# Positive	Total #	Percent Positive
Br SOLIS-ACE	0.57	109	113	96%
Br GONG-ACE	0.65	108	109	99%
Bt SOLIS-ACE	0.50	107	113	95%
Bt GONG-ACE	0.56	108	109	99%
Br SOLIS-Wind	0.57	111	115	97%
Br GONG-Wind	0.64	110	111	99%
Bt SOLIS-Wind	0.50	108	115	94%
Bt GONG-Wind	0.57	110	111	99%

percentage of static flux required to provide a one-to-one correlation match to the normal field strength observed at 1 AU. Figure 6 shows that our nominal use of these falloff values with a 2% amount of SOLIS magnetogram input required to provide closed-field extrapolations from 1.3 Rs height for the sample Carrington rotation 2056 used here. We note for this time that the GONG inputs do not provide adequate flux at 1.0 AU for a good match and must be increased by a factor of about 2 to get a similar match relative to the SOLIS data. Tangential fields alone from SOLIS multiplied by a factor of ~2.5 at the source surface, and from there decreased like the radial component, again provide the tangential field variations at Earth. These tangential fields do not include closed source-surface radial fields that could provide an additional component of the tangential field from the second equation in Figure 2.

The CSSS closed-field analysis for Carrington rotation 2056 shows something very striking. The radial closed fields from 1.3 Rs give an even better correlation with values measured in situ than the CSSS open-field analyses do. The φ or tangential (Bt) component values also give a weakly positive correlation. Additionally, and most importantly, the θ, normal (Bn), or north-south component also gives a significant positive correlation for this rotation. We further explore this type of analysis and the ability to mix results from different modeling techniques for Carrington rotation 2056, in section 5 (discussion) of the present article.

The main thrust of the present article is an exploration of the different data sets used in these magnetic field studies. For this we use the analyses described above to provide a survey of these two different types of both open- and closed-field CSSS analyses and the ability of NSO SOLIS and GONG magnetograms to provide low-resolution component radial and tangential fields at Earth. The next two sections present these comparisons with data from both ACE and Wind.

3. CSSS Open-Field Model Analysis Using SOLIS and GONG Magnetograms

We have used SOLIS magnetogram data sets [*Keller et al.*, 2003a, 2003b] in our extrapolations since they were available. Magnetograms termed "svsm_m11lr_B3_cr*.fts" are obtained over time and merged with a

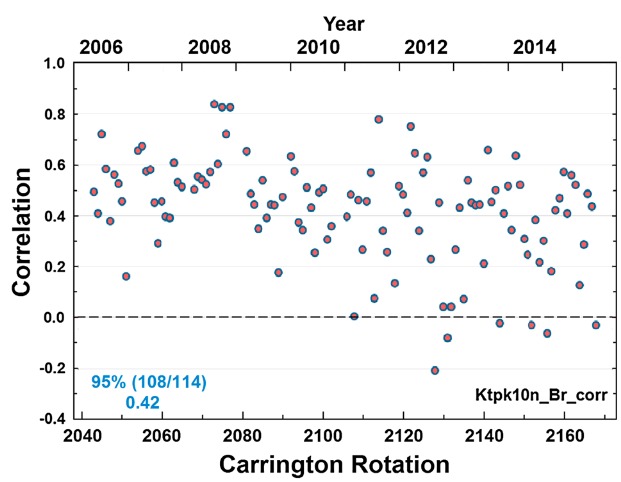

Figure 11. Correlations for the radial (Br) field from CSSS closed-field SOLIS analysis extrapolated to Earth and compared with ACE in situ observations.

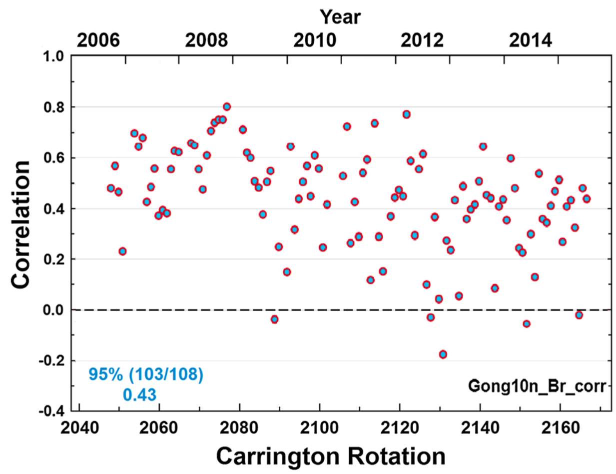

Figure 12. Correlations for the radial (Br) field from CSSS closed-field GONG analysis extrapolated to Earth and compared with ACE in situ observations.

weighted longitude sum within about 60° longitude of the Earth's central meridian. Magnetogram maps are available daily (weather permitting) from magnetograms obtained at Kitt Peak and more recently from the same instrument moved to "the farm" off the peak; they provide a consistent set of reliable observations over the 10 year period. Occasionally, these are incompletely filled and our software usually removes these from the record. We precondition our CSSS-model analyses of them to reduce bad areas. Blank areas on the CSSS-provided maps are filled with a spherical-surface Gaussian interpolation. We make maps at the intervals of the tomographic temporal analysis and, following their production, interpolate the CSSS-provided maps with a two-dimensional spline filter designed to show transient variations between maps rather than average these differences. This can lead to overemphasized noise in a sequence of closely spaced maps, and for this reason we now reject extra maps obtained only a few hours apart on the same day.

GONG-merged magnetograms (see http://gong.nso.edu/data/magmap/) used in the UCSD analysis termed "mrbqs*c*.fts" are currently treated in the same way as the SOLIS maps. These maps are smoothed by the NSO over periods of several days to reduce noise, and this in turn decreases the sensitivity of the maps to rapid transient variations. These maps available in 2006 at a cadence of two per day have more recently become available at a higher cadence. We now download these with an approximate 6 h cadence, which is adequate for our low-resolution study. We have also experimented with using NSO GONG *Janus* maps where no such few day averaging is made prior to their being available.

Figures 7–10 show the correlations from extrapolations of the CSSS open-field model SOLIS and GONG values of radial and tangential field over the 10 years since they were first available compared with ACE

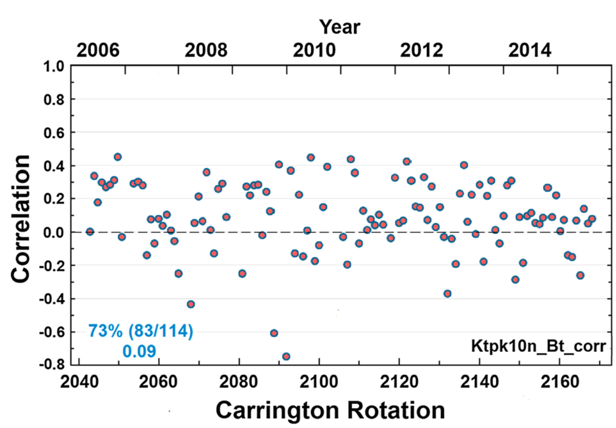

Figure 13. Correlations for the tangential (Bt) field from CSSS closed-field SOLIS analysis extrapolated to Earth and compared with ACE in situ observations.

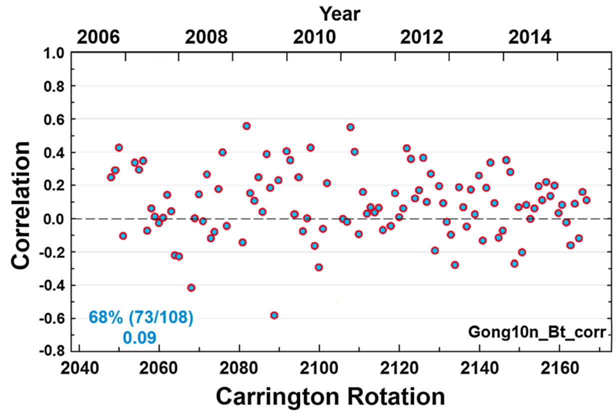

Figure 14. Correlations for the tangential (Bt) field from CSSS closed-field GONG analysis extrapolated to Earth and compared with ACE in situ observations.

magnetometer measurements. We find that slightly higher correlations at Earth are obtained when the 3-D tomographic reconstruction analysis is operated at 10° × 10° latitude and longitude and half a day temporal cadence, and thus, we have used this better resolution throughout our analysis. Additionally, the tomography was matched with Wind measurements throughout, because over the 10 year time period these give a more consistent result than the ACE level-0 measurements do, especially for densities. ACE level 2 data are also available and can be used in these analyses, but these data sets are not complete, especially during CMEs for some Carrington rotations, and thus, we have not used them regularly. Each figure also has a summary of the number of positive correlation values and an average of all correlations. Thus, for instance, in Figure 7, 109 of 113 total or 96% of the Carrington rotation correlations were positive, and the average correlation of all entries was 0.57.

Our study was more comprehensive than just Figures 7–10 and also compared the 3-D tomography analyses with Wind magnetic field measurements. Wind gave somewhat different results than the ACE comparisons. Table 1 provides a summary.

4. CSSS Closed-Field Model Analysis Using SOLIS and GONG Magnetograms

The closed-field analyses from the CSSS modeling was also tested over the 10 year period. We performed this analysis with both SOLIS and GONG magnetogram data sets as in sections 2 and 3 using a radial propagation of the field from 1.3 Rs and compared these with both ACE level 0 and Wind data sets. Again, the 3-D tomography was run with a 10° × 10° latitude and longitude spatial resolution and half a day temporal cadence, and the tomography was matched with Wind velocity and density measurements throughout. Both SOLIS and GONG magnetogram data were treated and preconditioned in the same way as were those used in the CSSS open-field analysis, and both were interpolated for the tomographic analysis with our spline filtering technique. Figures 11–14 show the comparisons of these closed-field analyses compared with ACE level 0 measurements. The correlations with both ACE and Wind (not shown in figures) magnetic field measurements were determined, and these summaries are given in Table 2.

Table 2. CSSS Closed-Field Model Extrapolation and Correlation Comparison

Comparison	Average Correlation	# Positive	Total #	Percent Positive
Br SOLIS-ACE	0.42	108	114	95%
Br GONG-ACE	0.43	103	108	95%
Bt SOLIS-ACE	0.09	83	114	73%
Bt GONG-ACE	0.09	73	108	68%
Br SOLIS-Wind	0.42	110	115	97%
Br GONG-Wind	0.42	107	110	97%
Bt SOLIS-Wind	0.08	79	115	69%
Bt GONG-Wind	0.08	76	110	69%

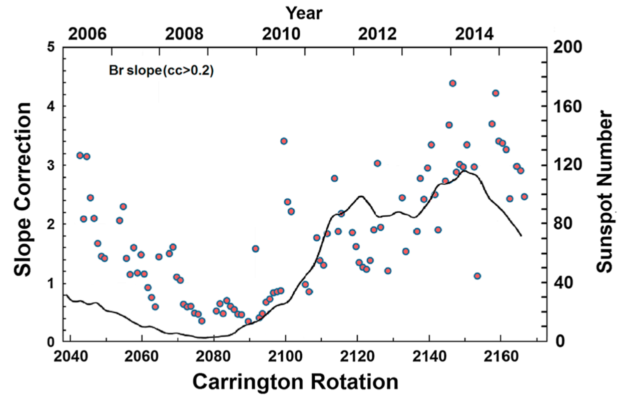

Figure 15. Slope correction needed to provide a one to one correlation for the CSSS closed-field SOLIS analysis and the radial (Br) field component extrapolated to Earth and compared with ACE in situ observations. Only positive correlations >0.2 are shown. The solar sunspot number is superimposed on the plot as a continuous line.

Of interest here is the difference in the percentage of static flux required to provide a one-to-one relationship with the measurements at ACE or Wind. This varied over the 10 year interval observed and can be represented as a "slope correction" or multiplier for the extrapolated fields required to match in situ measured fields. Figures 15–19 show this variation over the 10 year period for the closed-field extrapolations of both the SOLIS and GONG data sets. Slope corrections over the 10 year period of the same magnitude were also noted for the Wind comparisons (the plot of slope corrections for radial field and GONG data using Wind in situ measurements is shown in Figure 17), and thus, these changes have little to do with ground or space-based instrument calibrations. The corrections show that the amount of escaping flux provided by the Sun to produce a one-to-one correlation must be lessened gradually over time and is especially smaller at the end of the 10 year period relative to the period from 2008 to 2009. This indicates that the process of mass expulsion for closed fields becomes more efficient at the beginning and end of the 10 year period. In the slope correction comparison with ACE magnetogram data of Figure 15, we plot the smoothed monthly sunspot number over the same period as obtained from http://sidc.be/silso/datafiles. This is discussed in the next section.

5. Discussion

The CSSS open-field analyses presented in section 3 show significantly better correlations during the 10 year period in the GONG data set for both the radial and tangential fields than the SOLIS data sets do. Although

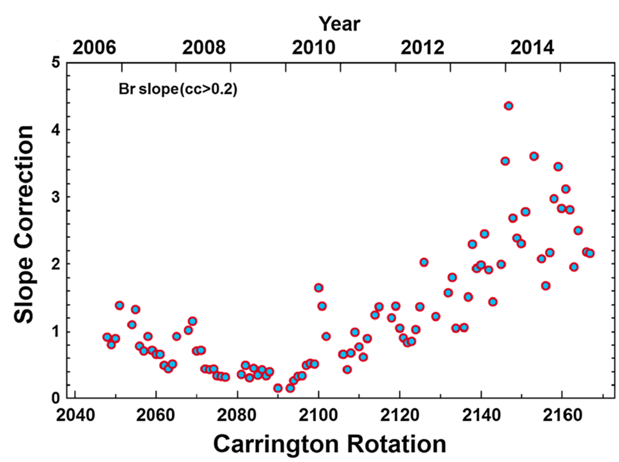

Figure 16. Slope correction needed to provide a one to one correlation for the CSSS closed-field GONG analysis and the radial (Br) field component extrapolated to Earth and compared with ACE in situ observations. Only positive correlations >0.2 are shown.

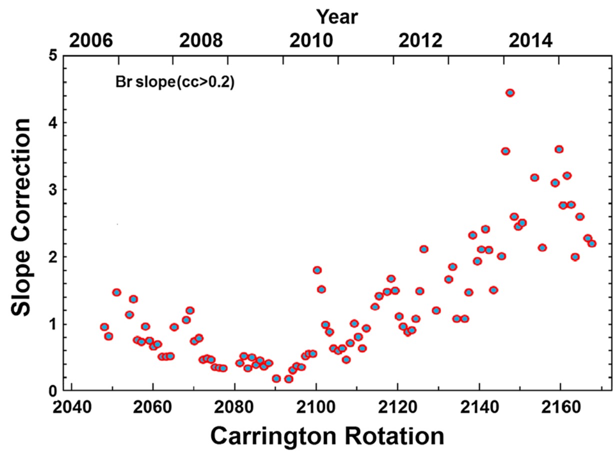

Figure 17. Slope correction needed to provide a one-to-one correlation for the CSSS closed-field GONG analysis and the radial (Br) field component extrapolated to Earth and compared with Wind in situ observations. Only positive correlations >0.2 are shown.

the excursions are always greater and usually much higher than 0.4 nT from the mean, for both modeled and in situ values in each Carrington rotation, we did not use a lower limit to eliminate those rotations with smaller changes in field. In our analyses it is generally unfeasible to check each magnetogram for strange features, and we may have incompletely edited or not removed every bad (incomplete, noisy, file with wrong headers, etc.) magnetogram as intended. Even a single bad magnetogram can place a large excursion in the data in the tomographic analysis, and this is a potential reason for poor correlations in any given Carrington rotation that might bring down the average over the 10 year period. Carefully edited data sets in individual rotations often provide as good results from SOLIS magnetograms. Thus, it is not clear whether the better GONG correlations are simply a matter of having more magnetograms at a regular cadence in the analysis, as the GONG data allow. Some periods show poor correlations and even negative correlations from both magnetogram data sets such as those near Carrington rotation 2090. We can find no cause for this in the 3-D reconstruction analysis. A slight trend shows a correlation-coefficient decrease at the end of the 10 year period, and this may be caused by the generally greater amount of activity at the maximum of the solar cycle. We find no obvious daily lag or lead shift at the low temporal resolutions explored between the tomographically derived fields that are assumed to corotate up to 15 Rs and then are extrapolated radially outward from the Sun.

The ACE magnetometers are flight spares originally designed for the Wind spacecraft, and so one would expect these to provide results similar to those from Wind since both spacecraft are near the L_1 Lagrange

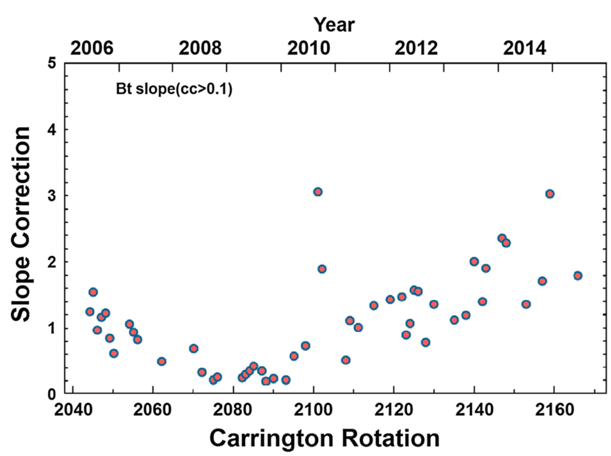

Figure 18. Slope correction needed to provide a one-to-one correlation for the CSSS closed-field SOLIS analysis and the tangential (Bt) field component extrapolated to Earth and compared with ACE in situ observations. Only positive correlations >0.1 are shown.

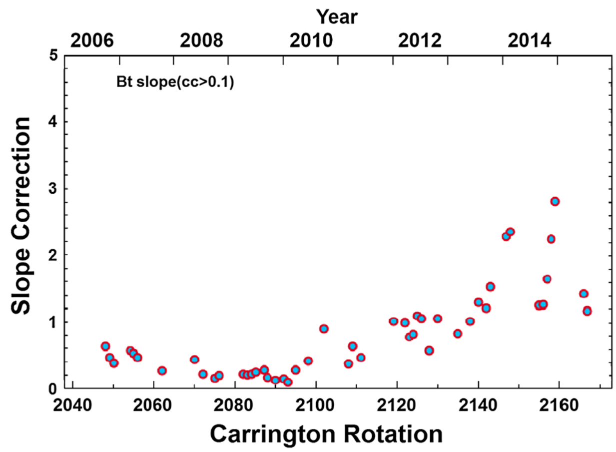

Figure 19. Slope correction needed to provide a one to one correlation for the CSSS closed-field GONG analysis and the tangential (Bt) field component extrapolated to Earth and compared with ACE in situ observations. Only positive correlations >0.1 are shown.

point sunward of the Earth. This is especially the case at these low resolutions since the heliospheric structures measured are smoothed to very large sizes and not dependent on the small differences of the spacecraft orbits. Nevertheless, there are differences, and these are probably instrumental in origin, as can often be observed in detailed comparisons of their data sets. Overall, however, there is little difference in the final percentages and numbers of good and bad correlations, and both in situ data sets show the same change in slope over the 10 year period of the comparisons.

It is surprising that the closed-field analyses from 1.3 Rs shown in section 4 give such good results for radial (Br) fields. That the field at 1.3 Rs has a radial component observed near 1 AU with the same sign in the interplanetary medium probably should be expected since this field can come directly out of the Sun to reach Earth. However, it was unexpected that the correlations from these low fields could be so good and, in fact, even superior at times (such as in the sample Carrington rotation 2056 shown in section 2) to the fields of the CSSS open-field analyses that are gathered by the modeling and presented on the tomography source surface from photospheric locations far beyond those sub-Earth. However, over the 10 year period, these radial fields do not show better correlations than those from the CSSS open-field analysis. The radial closed field correlations show a gradual decrease over time, and this may be caused by the increased solar activity at the end of the 10 year period. The closed-field average differences between the GONG and SOLIS data sets show that neither data set provides a clearly superior result relative to in situ measurements at 1 AU unlike the open-field analyses. Since the same magnetogram data were used in both the open- and closed-field analyses and the closed-field analysis provides information from a location closer to the sub-Earth point, we speculate that both data sets are probably equally accurate near the sub-Earth point. It is most likely that data set interpolation and editing (either ours, as stated before, or the way data sets are combined by the NSO for the less numerous SOLIS magnetograms) explains the superior result for the GONG data set used in the CSSS model open-field analyses.

It is more surprising that the tangential (Bt) and some normal (Bn) field comparisons show a positive correlation. For the tangential fields this correlation is persistent, if only weakly correlated, throughout the 10 year study period. Because of the need to explore these effects more completely, we recently revised our programming so both closed and open fields can be mixed. This presumes that there are two processes providing the fields observed near Earth: one that gathers fields far from the sub-Earth location and another that more directly incorporates radial propagating fields. Figure 20 shows the result of this analysis for our sample Carrington rotation 2056 using the GONG data. Figure 20a mixes both the CSSS radial open and closed fields equally, and when this is done the result is a higher correlation than either provide separately. The tangential fields show the same effect. In the analysis shown, the combination of the two radial components through the second equation of Figure 2 provides about the same correlation as the closed component does singly (Figure 20b). The correlation for tangential field employing the radial field component through the second equation of Figure 2 has a correlation of 0.682 and is not shown. When the closed tangential field is added to both of the others in an equal amount, the correlation coefficient becomes even better as shown in Figure 20c. Since the normal (Bn) component in our analysis has no relationship to the other two, it is unchanged from Figure 6c and thus is not shown.

Slope correction changes with time for the closed-field analyses are of interest since this is likely an indicator of a possible mechanism for the closed-field expulsion. It is very unlikely to be an instrumental effect since both SOLIS and GONG magnetograms show the same effect whether compared either with ACE or with

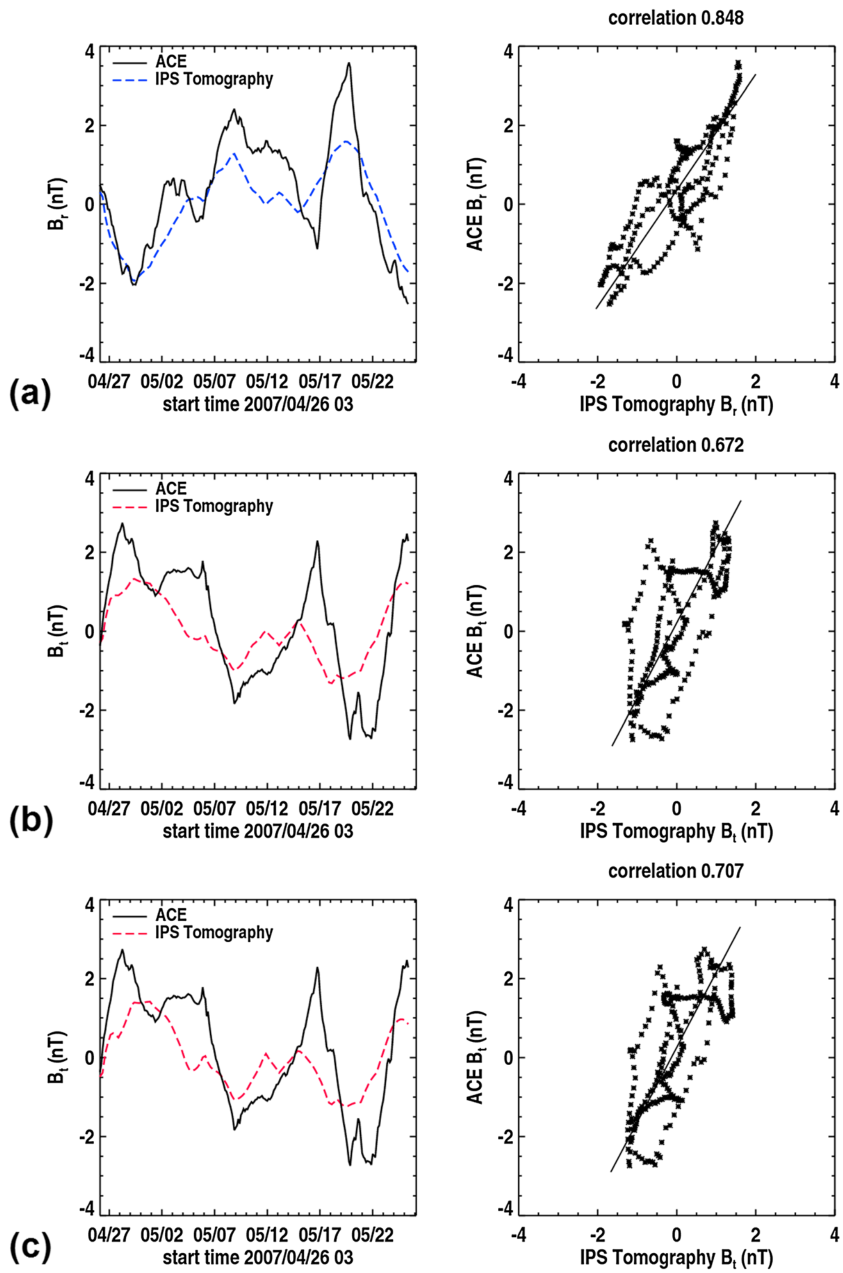

Figure 20. Time series (left) and correlations (right) from a combination of the CSSS open-field modeling and the CSSS closed-field modeling at 1.3 Rs and IPS 3-D reconstruction extrapolations of GONG data compared with ACE magnetometer measurements over the Carrington rotation 2056 time period. As in Figure 6 the in situ measurements have been smoothed by a 3 day "boxcar" filter to provide a signal commensurate with the smoothed measurements from the CSSS modeling. (a) Radial fields supplied in equal quantities at half the amplitude of either that provided the radial fields of Figures 5a and 6b. (b) Tangential fields provided as a combination of both the radial components as in Figure 5b and from the radial field of Figure 6a combined in equal amounts. (c) Tangential fields provided as a combination of both the radial components and the tangential component of Figure 6b, with all three provided in equal amounts at the source surface.

Wind in situ measurements. The slope corrections amount to a factor of ~3 difference from the mean value in any given year during the 10 year time interval. No such variation over time is observed in the CSSS model open-field analyses to within ~20% of the mean value. This was also shown in *Zhao and Hoeksema* [1995] for the CSSS model for a 9 year period from 1977 to 1985 through the solar cycle 21 maximum; this constancy indicates that over the 10 year period we analyzed that what is observed in photospheric fields is proportionally the same as in space, and thus, the mechanism providing the flux near Earth is responsible for the slope

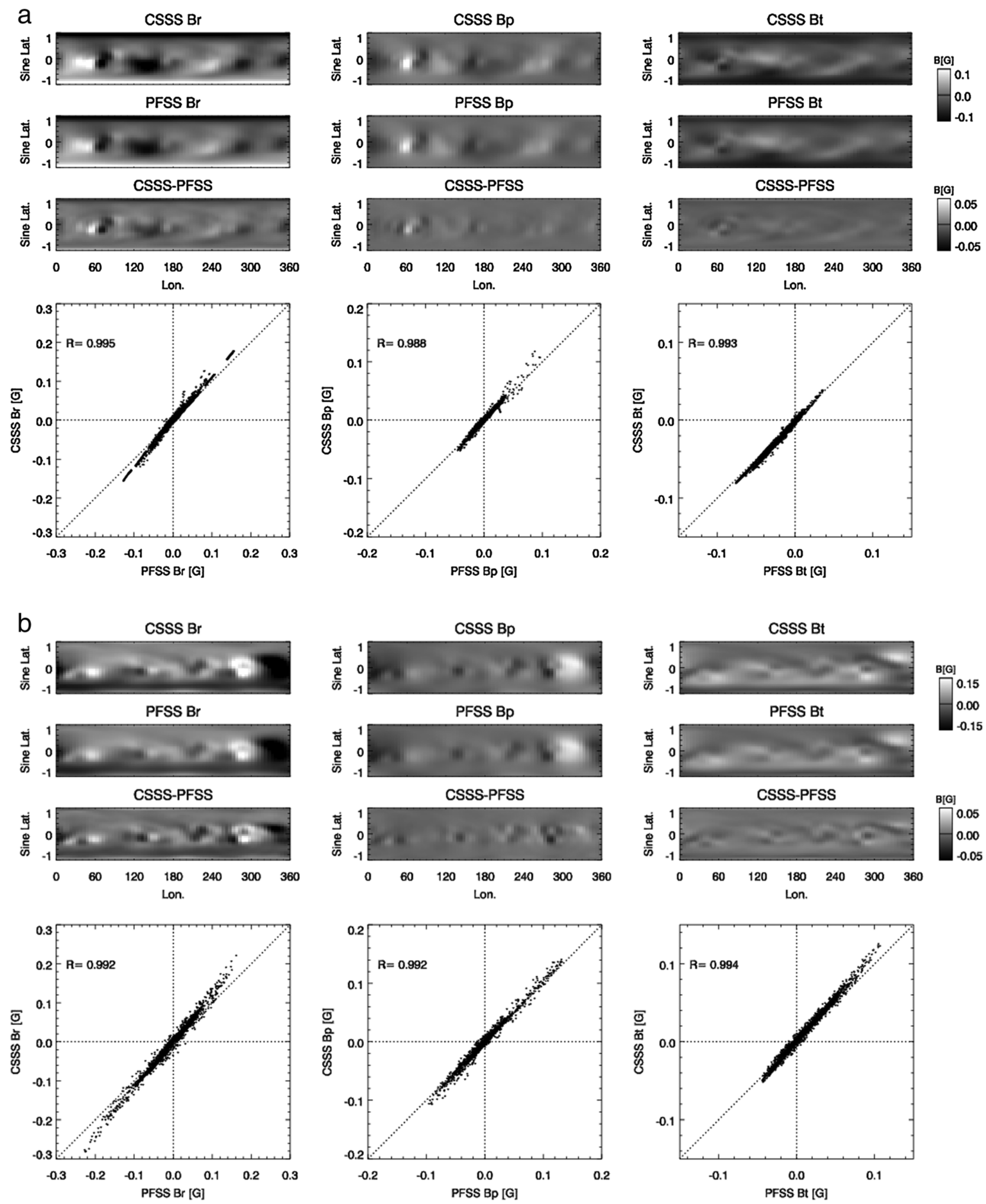

Figure 21. (a) Comparison of the three closed-field components from both the PFSS and CSSS models at 1.3 Rs for SOLIS magnetogram 2056.242 (Carington rotation; fraction in degrees) in 2007. (b) Comparison of the three closed-field components from both the PFSS and CSSS models at 1.3 Rs for SOLIS magnetogram 2169.180 in 2015.

correction required. We show the sunspot number on Figure 15: with a lag of about 1 year, the CSSS closed-field slope corrections show fairly good agreement. We thus speculate that it is most likely that the closed-field expulsion has something to do with level of solar activity, perhaps associated with CMEs, but more likely simply the stronger magnetic fields near the solar equator over the solar cycle. For space weather forecasts this variation over solar cycle needs to be accounted for when using this technique to map closed fields to Earth.

We also attempted using GONG *Janus* maps for a subset of the data in 2007 and in 2015, to determine if the higher cadence of nonsmoothed merged magnetograms gave a better result in our analyses. Tomographic analyses using *Janus* data had larger variations during these two test years. However, for these two periods we found, in general, that the results had no better correlations for the extrapolations of the CSSS open-field model radial, tangential, and CSSS closed-field radial, tangential, and normal fields. Thus, we did not pursue this particular approach further.

We also have been interested to find differences between the closed fields of the CSSS model and the PFSS model. Any potential difference in the two modeled fields is quickly discovered by using the same magnetogram and then comparing radial, tangential, and normal component maps from both models. The PFSS model, like the CSSS model, has a long heritage [*Hakamada*, 1995]. Figures 21a and 21b show examples of this comparison of the two modeling techniques at two times in the solar cycle: respectively, SOLIS magnetogram 2056.242 in 2007 at solar minimum and from 2169.180 in 2015 at solar maximum. Both models have nearly identical maps of closed-field structures in this test case obtained at 1.3 Rs. The $n = 20$ expansion coefficients as in earlier sections of this article were employed. Closed components viewed for these two time periods, and at a variety of different heights from the Sun, give the same closed-field structures generally within a few percent and never more than 20% from each model, anywhere in the maps. Thus, in summary, there is little difference in the CSSS model relative to the PFSS model for providing closed fields in these analyses.

A more complete analysis of the normal (Bn) component is beyond the scope of the current article, and not discussed further here, except to say that all parties involved in this current study retain an interest in it. This is the most important component to determine regularly, since it is the dominant field that couples with the Earth's magnetic field to generate geomagnetic storm and substorm activity [*Kamide et al.*, 1997]. Current analyses over the 10 years show that some rotations provide good correlations while others do not; we continue to explore the reasons for this and are guided by the fact that a combination of both the closed sub-Earth fields and fields distant from this provides better correlations than either one does singly. Additionally, there is the matter of which closed height gives the best correlations overall and how many modeling coefficients and thus which coronal structure sizes contribute the most to the closed-field extrapolations.

6. Conclusion

We have analyzed NSO SOLIS and GONG magnetograms using the CSSS model and UCSD 3-D reconstruction tomography to provide both open- and closed-field analyses over a 10 year period since both were available. Pearson's R correlation systematically evaluates best analysis comparisons of these with both ACE and Wind magnetometer measurements in RTN coordinates. We find that the GONG results in these analyses generally provide slightly better comparisons for the open-field analyses, but it is not clear whether this is caused by better magnetometer measurements or by an inaccurate editing of these data sets.

For the closed field analyses both SOLIS and GONG data sets seem equally able to provide the same, if slightly less well correlated comparisons with radial fields near Earth. Although the tangential fields do not give good overall correlations over the 10 year period, the correlations are slightly positive. These correlations, and those of the normal fields, continue to be actively pursued in studies of their association with CMEs, and also the nonradial transport of the flux, especially near the surface of the Sun and through 3-D MHD heliospheric studies [see, e.g., *Jackson et al.*, 2015]. We note that in some instances, the correlations of the normal field for a single Carrington rotation can be fairly high (~0.7) [*Jackson et al.*, 2016], and in the case of mixing fields, both open and closed, which the combination can better the correlations than either taken singly.

An interesting result is the variation of the slope correction for closed fields over the 10 year period; the amount of flux released relative to that observed in situ varies by about a factor of 3 or more from a minimum at the end of 2008 to a maximum in 2014. This closed flux increase in efficiency relative to that observed in situ indicates a mechanism associated with increased sub-Earth solar magnetic field strengths near the maximum of the solar cycle. It takes energy to open closed loops, and we do not know the nature of this energy. However, because it seems to be associated with the strength of the magnetic field at the solar surface near its equator, we speculate that this is one of the factors involved. CMEs are one obvious solar cycle-dependent large-scale effect that could cause more closed flux to be transported from near the solar surface outward at solar maximum. Another more ubiquitous process could be that of the presumed Alfvén flux suggested by observations from the Coronal Multichannel Polarimeter [*Tomczyk et al.*, 2008].

Although slight differences occur in comparisons with ACE and Wind measurements for individual Carrington rotations, the correlation differences are negligible as an average over the present 10 year analysis interval. In a check at both solar minimum and solar maximum of the differences between the closed-component PFSS model and the CSSS model, we find that PFSS and CSSS model closed fields from the same magnetograms are nearly identical in sign and strength. This confirms, as expected, that both models provide the same lower coronal structure and that the currents added to the CSSS model used to open the field lines above the cusp surface have only a minimal effect below this solar distance.

We know of no other analyses that consistently provide better results for daily magnitudes of component magnetic fields determined on the solar surface compared to those measured in situ. Even so, the correlations we find are far from perfect, even at these relatively low temporal resolutions. We find many reasons for this, some of which have already been specified in the preceding pages of this article. First, there are measurement errors, both in magnetograms and how they are combined, and of the in situ field measurements. Both the CSSS and PFSS models are only approximate descriptions of coronal fields near the solar surface. The physics available with state-of-the-art models such as those that provide a 3-D MHD description of the corona and interplanetary medium are also incomplete, because many of the physical parameters required to link surface fields to in situ measurements are very difficult to observe. These physical parameters include the plasma temperature, the ratio of specific heats, and the coronal currents used to provide a portion of the field. In the inner interplanetary medium, the various energy generation and dissipation mechanisms and the plasma interactions that take place may not all be known or are not well observed. Moreover, getting the results from some state-of-the-art models tax even the largest computing facilities in order to provide their results. Thus, we are happy that this system works well enough to allow input for those who provide magnetic fields as well state-of-the-art modeling so that these efforts can be refined and used in space weather predictions and forecasts.

Acknowledgments
Jackson, H.-S. Yu, and A. Buffington have been partially funded by AFOSR contract FA9550-15-1-0477 and the US National Science Foundation contract AGS-1358399 to the University of California, San Diego. The Solar-Terrestrial Environment Laboratory (STELab, now ISEE), Japan, supported a portion of work on this project with partial funding for B.V. Jackson and H.-S. Yu during 2015–2016 from a laboratory-sponsored foreign visitor program. In addition, the ISEE IPS observations and ISEE authors carried out their studies for these analyses under the solar wind program of ISEE at Nagoya University. The UCSD programming that provides the tomographic analysis and the IDL visualizations including the field extrapolations and their display are online (http://cass.ucsd.edu/archive/solar/resources.html#resources), are also available at the NASA Goddard Coordinated Modeling Center, and are also updated weekly to SolarSoft. XuePu Zhao maintains a version of the CSSS model online (http://sun.stanford.edu/~xuepu/DATA/hccsss/). The IPS observations used in these analyses are available online (ftp://ftp.isee.nagoya-u.ac.jp/pub/vlist/). We thank the ACE spacecraft group for making their data available in real time for use at UCSD through the Space Weather Prediction Center, NOAA, Boulder, and to the Wind spacecraft group for making their data available (ftp://space.mit.edu/pub/plasma/wind/kp_files_hr_aves/).

References

Alfvén, H. (1942), Existence of electromagnetic-hydrodynamic waves, *Nature*, *150*, 405.

Arge, C. N., and V. J. Pizzo (2000), Improvement in the prediction of solar wind conditions using near-real time solar magnetic field updates, *J. Geophys. Res.*, *105*, 10,465–10,479, doi:10.1029/1999JA000262.

Dunn, T., B. V. Jackson, P. P. Hick, A. Buffington, and X. P. Zhao (2005), Comparative analyses of the CSSS calculation in the UCSD tomographic solar observations, *Sol. Phys.*, *227*, 339.

Hakamada, K. (1995), A simple method to compute spherical harmonic coefficients for the potential model of the coronal magnetic field, *Sol. Phys.*, *159*(1), 89.

Hewish, A., P. F. Scott, and D. Wills (1964), Interplanetary scintillation of small diameter radio sources, *Nature*, *203*, 1214.

Hick, P. P., and B. V. Jackson (2004), Heliospheric tomography: An algorithm for the reconstruction of the 3D solar wind from remote sensing observations, in *Proceedings of the SPIE*, vol. 5171, edited by S. Fineschi and M. A. Gummin, pp. 287, SPIE, Bellingham, Wash., doi:10.1117/12.513122.

Hoeksema, J. T., J. M. Wilcox, and P. H. Scherrer (1983), The structure of the heliospheric current sheet: 1978–1982, *J. Geophys. Res.*, *88*, 9910–9918, doi:10.1029/JA088iA12p09910.

Houminer, Z. (1971), Correlation of interplanetary scintillation and spacecraft plasma density measurements, *Nat. Phys. Sci.*, *231*, 165.

Hundhausen, A. J. (1972), *Solar Wind and Coronal Expansion*, 10 pp., Springer, New York.

Jackson, B. V., P. L. Hick, M. Kojima, and A. Yokobe (1998), Heliospheric tomography using interplanetary scintillation observations: 1. Combined Nagoya and Cambridge data, *J. Geophys. Res.*, *103*, 12,049–12,067, doi:10.1029/97JA02528.

Jackson, B. V., A. Buffington, and P. P. Hick (2001), A heliospheric imager for Solar Orbiter, in *Proc. of Solar Encounter: The First Solar Orbiter Workshop*, pp. 251–256, Santa Cruz de Tenerife, Spain.

Jackson, B. V., P. P. Hick, A. Buffington, M. Kojima, M. Tokumaru, K. Fujiki, T. Ohmi, and M. Yamashita (2003), Time-dependent tomography of heliospheric features using interplanetary scintillation (IPS) remote-sensing observations, in *Solar Wind Ten*, vol. 679, edited by M. Velli, R. Bruno, and F. Malara, 75 pp., Melville, New York.

Jackson, B. V., et al. (2004), The Solar Mass Ejection Imager (SMEI) mission, *Sol. Phys.*, *225*, 177.

Jackson, B. V., P. P. Hick, A. Buffington, M. M. Bisi, J. M. Clover, and M. Tokumaru (2008), Solar Mass Ejection Imager (SMEI) and Interplanetary Scintillation (IPS) 3D-reconstructions of the inner heliosphere, *Adv. Geosci.*, *21*, 339.

Jackson, B. V., P. P. Hick, M. M. Bisi, J. M. Clover, and A. Buffington (2010), Inclusion of in-situ velocity measurements in the UCSD time-dependent tomography to constrain and better-forecast remote-sensing observations, *Sol. Phys.*, *265*, 245, doi:10.1007/s11207-010-9529-0.

Jackson, B. V., P. P. Hick, A. Buffington, M. M. Bisi, J. M. Clover, M. Tokumaru, M. Kojima, and K. Fujiki (2011), Three-dimensional reconstruction of heliospheric structure using iterative tomography: A review, *J. Atmos. Sol. Terr. Phys.*, *73*, 1214.

Jackson, B. V., P. P. Hick, A. Buffington, J. M. Clover, and M. Tokumaru (2012), Forecasting transient heliospheric solar wind parameters at the locations of the inner planets, *Adv. Geosci.*, *30*, 93.

Jackson, B. V., J. M. Clover, P. P. Hick, A. Buffington, M. M. Bisi, and M. Tokumaru (2013), Inclusion of real-time in-situ measurements into the UCSD time-dependent tomography and its use as a forecast algorithm, *Sol. Phys.*, *285*, 151.

Jackson, B. V., et al. (2015), The UCSD IPS solar wind boundary and its use in the ENLIL 3D-MHD prediction model, *Space Weather*, *13*, 104–115, doi:10.1002/2014SW001130.

Jackson, B. V., et al. (2016), Using world interplanetary scintillation systems for space weather predictions, oral presentation at the PSTEP Symposium Conference, Nagoya, Japan, 13–15 Jan.

Kamide, Y., R. L. McPherron, W. D. Gonzalez, D. C. Hamilton, H. S. Hudson, J. A. Joselyn, S. W. Kahler, L. R. Lyons, H. Lundstead, and E. Szuszczewicz (1997), Magnetic storms: Current understanding and outstanding questions, in *Magnetic Storms*, *Geophys. Monogr.*, edited by B. T. Tsurutani et al., p. 1 , AGU, Washington, D. C.

Keller, C. U., J. W. Harvey, M. S. Giampapa, and the SOLIS Team (2003a), SOLIS: An innovative suite of synoptic instruments, *Proc. SPIE*, *4853*, 194.

Keller, C. U., J. W. Harvey, and SOLIS Team (2003b), The SOLIS vector-spectromagnetograph, in *Solar Polarization 3*, edited by J. Trujillo-Bueno and J. Sanchez-Almeida, pp. 13, Astronomical Society of the Pacific, San Francisco, Calif.

Kojima, M., and T. Kakinuma (1987), Solar cycle evolution of solar wind speed structure between 1973 and 1985 observed with the interplanetary scintillation method, *J. Geophys. Res.*, *92*, 7269–7279, doi:10.1029/JA092iA07p07269.

Kojima, M., M. Tokumaru, H. Watanabe, A. Yokobe, K. Asai, B. V. Jackson, and P. L. Hick (1998), Heliospheric tomography using interplanetary scintillation observations: 2. Latitude and heliocentric distance dependence of solar wind structure at 0.1–1 AU, *J. Geophys. Res.*, *103*, 1981–1989, doi:10.1029/97JA02162.

Mackay, D. H., and A. R. Yeates (2012), The Sun's global photospheric and coronal magnetic fields: Observations and models, *Living Rev. Sol. Phys.*, *9*, 6, doi:10.12942/lrsp-2012-6.

Mariani, F., and F. M. Neubauer (1990), The interplanetary magnetic field, in *Physics of the Inner Heliosphere: 1. Large-Scale Phenomena*, *Phys. and Chem. in Space and Sol. Phys.*, vol. 20, edited by M. C. E. Huber, L. J. Lanzerotti, and D. Stoffler, 183 pp., Springer, Berlin.

McComas, D. J., S. J. Bame, P. Barker, W. C. Feldman, J. L. Phillips, P. Riley, and J. W. Griffee (1998), Solar Wind Electron Proton Alpha Monitor (SWEPAM) for the advanced composition explorer, *Space Sci. Rev.*, *86*, 563.

Nishimura, N., N. Nozaki, B. V. Jackson, H.-S. Yu, M. Tokumaru, K. Fujiki, and K. Hakamada (2016), Comparison of calculated and observed IMF near magnetic cloud start times, paper presented at the Japan Geophysical Union Meeting, Makuhari, Japan, 22–23 May.

Nozaki, N., N. Nishimura, B. V. Jackson, H.-S. Yu, M. Tokumaru, K. Fujiki, K. Hayashi, and K. Hakamada (2016), A statistical study of the radial and north-south component values of heliospheric magnetic field, paper presented at the Japan Geophysical Union Meeting, Makuhari, Japan, 22–23 May.

Ogilvie, K. W., and G. K. Parks (1996), First results from WIND spacecraft: An introduction, *Geophys. Res. Lett.*, *23*, 1179–1181, doi:10.1029/96GL01357.

Owens, M. J., N. U. Crooker, N. A. Schwadron, T. S. Horbury, S. Yashiro, H. Xie, O. C. S. Cyr, and N. Gopalswamy (2008), Conservation of open solar magnetic flux and the floor in the heliospheric magnetic field, *Geophys. Res. Lett.*, *35*, L20108, doi:10.1029/2008GL035813.

Press, W. H., B. P. Flannery, S. A. Teukolsky, and W. T. Vetterling (1988), Numerical Recipes The Art of Scientific Computing, Cambridge Univ., Press, Cambridge, Mass.

Riley, P., R. Lionello, J. A. Linker, Z. Mikic, J. Luhmann, and J. Wijaya (2011), Global MHD modeling of the solar corona and inner heliosphere for the whole heliosphere interval, *Sol. Phys.*, *274*, 361, doi:10.1007/s11207-010-9698-x.

Russell, C. T. (2001), Solar wind and interplanetary magnetic field: A tutorial, in *Space Weather*, *Geophys. Monogr. Ser.*, vol. 125, edited by P. Song, H. J. Singer, and G. L. Siscoe, 73 pp., AGU, Washington D. C.

Schatten, K. H., J. W. Wilcox, and N. E. Ness (1969), A model of interplanetary and coronal magnetic fields, *Sol. Phys.*, *6*, 442.

Stone, E. C., A. M. Frandsen, R. A. Mewaldt, E. R. Christian, D. Margolies, J. F. Ormes, and F. Snow (1998), The advanced composition explorer, *Space Sci. Rev.*, *86*, 1.

Tokumaru, M. (2013), Three-dimensional exploration of the solar wind using observations of interplanetary scintillation, *Proc. Jpn. Acad., Ser. B*, *89*, 67.

Tomczyk, S., G. L. Card, T. Darnell, D. F. Elmore, R. Lull, P. G. Nelson, K. V. Streander, J. Burkepile, R. Casini, and P. G. Judge (2008), An instrument to measure coronal emission line polarization, *Sol. Phys.*, *247*, 411.

Wu, C.-C., K. Liou, B. V. Jackson, H.-S. Yu, L. Hutting, R. P. Lepping, S. Plunkett, R. A. Howard, and D. Socker (2015a), The first super geomagnetic storm of solar cycle 24: "The St. Patrick day (17 March 2015)" event, paper presented at the SCOSTEP-WDS Workshop, NICT, Tokyo, Japan, 28–30 Sept.

Wu, C.-C., K. Liou, D. Socker, R. A. Howard, B. V. Jackson, H.-S. Yu, L. Hutting, and S. Plunkett (2015b), The first super geomagnetic storm of solar cycle 24: "The St. Patrick day (17 March 2015)" event, Abstract SH51A-2433 presented at 2015 Fall Meeting, AGU, San Francisco, Calif., 14–18 Dec.

Yeates, A. R., D. H. Mackay, A. A. van Ballegooijen, and J. A. Constable (2010), A nonpotential model for the Sun's open magnetic flux, *J. Geophys. Res.*, *115*, A09112, doi:10.1029/2010JA015611.

Yu, H.-S., B. V. Jackson, P. P. Hick, A. Buffington, D. Odstrcil, C.-C. Wu, J. A. Davies, M. M. Bisi, and M. Tokumaru (2015), 3D reconstruction of Interplanetary Scintillation (IPS) remote-sensing data: Global solar wind boundaries for driving 3D-MHD models, *Sol. Phys.*, *290*, 2519, doi:10.1007/s11207-015-0685-0.

Zhao, X., and J. T. Hoeksema (1995), Prediction of the interplanetary magnetic field strength, *J. Geophys. Res.*, *100*, 19–33, doi:10.1029/94JA02266.